

1 **Effect of Site-disorder, Off-stoichiometry and Epitaxial Strain on the**
2 **Optical Properties of Magnetolectric Gallium Ferrite**

3
4 Amritendu Roy¹, Somdutta Mukherjee², Surajit Sarkar², Sushil Auluck³, Rajendra
5 Prasad², Rajeev Gupta^{2,4} and Ashish Garg^{1*}

6
7 ¹Department of Materials Science & Engineering, Indian Institute of Technology,
8 Kanpur-208016, India

9 ²Department of Physics, Indian Institute of Technology, Kanpur - 208016, India

10 ³National Physical Laboratory, Dr. K. S. Krishnan Marg, New Delhi-110012, India

11 ⁴Materials Science Programme, Indian Institute of Technology, Kanpur - 208016, India

12
13 **ABSTRACT**

14
15 We present a combined experimental-theoretical study demonstrating the role of site
16 disorder, off-stoichiometry and strain on the optical behavior of magnetolectric gallium
17 ferrite. Optical properties (band-gap, refractive indices and dielectric constants) were
18 experimentally obtained by performing ellipsometric studies over the energy range 0.8 –
19 4.2 eV on pulsed laser deposited epitaxial thin films of stoichiometric gallium ferrite with
20 *b*-axis orientation and the data was compared with theoretical results. Calculations on the
21 ground state structure show that the optical activity in GaFeO₃ arises primarily from O2p-
22 Fe3d transitions. Further, inclusion of site disorder and epitaxial strain in the ground state
23 structure significantly improves the agreement between the theory and the room
24 temperature experimental data substantiating the presence of site-disorder in the
25 experimentally derived strained GaFeO₃ films at room temperature. We attribute the
26 modification of the ground state optical behavior upon inclusion of site disorder to the
27 corresponding changes in the electronic band structure, especially in Fe3d states leading
28 to a lowered band-gap of the material.

29
30
31 **Keywords:** Gallium ferrite, thin films, optical properties, ellipsometry, first-principles
32 calculation

33
34
35 **PACS No.:** 78.20.-e, 77.55.Nv, 71.15.Mb

36
37
38

* Corresponding author, Tel: +91-512-2597904; FAX - +91-512-2597505, E-mail: ashishg@iitk.ac.in

1 I. Introduction

2
3 Optical properties of piezoelectric and ferroelectric oxides have been of interest for a
4 variety of applications [1-4] ranging from optical waveguides, [2] photocatalysis, [5] and
5 infrared detection [3, 4] to more recently photovoltaics. [6, 7] As an additional degree of
6 freedom in many of these materials such as magnetoelectrics and multiferroics,
7 magnetism often yields a reduced band gap [8, 9], enhancing their suitability for
8 photovoltaic applications. Further, tunability of the band gap *vis-à-vis* electronic structure
9 in these materials could be accomplished by tailoring the crystal structure where external
10 perturbations such as doping [10] and strain [11] play crucial role in determining
11 structural symmetry as well as physical properties *e.g.* optical properties. To fabricate
12 efficient optical devices, it is essential to understand the microscopic effects of such
13 perturbations *vis-à-vis* their contributions to the electronic structure as well as optical
14 properties. In this regard, first-principles density functional theory (DFT) based studies
15 have been quite successful in predicting and analyzing the ground state as well as
16 electronic structure and optical properties of complex oxide systems. [12, 13] The
17 disadvantage of underestimation of electronic band gap by conventional LDA and GGA
18 functionals [14, 15] of DFT could be avoided by suitably scaling the calculated results
19 with the experimental observations.

20 We have chosen to study the optical properties of gallium ferrite (GaFeO_3 or
21 GFO) which is a prospective room temperature magnetoelectric with comparatively small
22 band gap ($\sim 2.5\text{-}3$ eV) [14, 16] and therefore, attractive for potential photovoltaic
23 applications. Further, GFO exhibits a number of exciting optical phenomena such as
24 optical magnetoelectric effect, [17, 18] and magnetization induced non-linear second
25 harmonic Kerr effect. [19, 20] The observed ferrimagnetism, which can be tuned by
26 tailoring the Ga:Fe ratio [21, 22] and processing conditions, [21-23] is believed to be the
27 manifestation of inherent cation site disorder [21, 24] emanating from almost similar
28 sizes of Fe and Ga. Previous optical studies on GFO single crystals [25] and thin films
29 [16] using ellipsometry and absorption studies showed red-shift of the fundamental
30 absorption edge with increasing Fe content. However, microscopic origin of such red-
31 shift is rather generalized and one needs to decouple the possible contributions of external
32 factors such as Fe content, cationic site disorder and epitaxial strain to completely
33 understand the optical response of the material. In this context, systematic first-principles
34 calculations along with appropriate experimental data could provide an atomistic insight
35 into optical response of the material.

36 In this paper, we present the results of a combined experimental and theoretical
37 study of the linear optical properties of GFO. Epitaxial thin films of GFO were chosen
38 specifically to understand the combined effects of inherent cation site disorder as well as
39 epitaxial strain on its optical properties which were decoupled using first-principles'
40 calculations. Our calculations show that the inter-band transitions, responsible for optical
41 activities of GFO are primarily due to O2p-Fe3d transitions. More importantly, we
42 clearly observe that incorporation of cation site disorder and epitaxial strain into the
43 ground state structure yields a much improved agreement between the theoretical
44 predictions and experimental observations substantiating the role of cation site disorder
45 which is explained in terms of modification of the Fe 3d bands. Subsequent parts of the
46 paper are organized as follows: section II discusses the experimental techniques and

1 calculation methodologies used in the study, section III presents the results of both
2 ellipsometric measurements and first-principles calculations on the ground state structure
3 along with external effects such as disorder, strain, off-stoichiometry and hydrostatic
4 pressure and section IV summarizes the manuscript.

5 6 7 **II. Experimental and Calculation Details**

8
9 GFO thin films were grown using pulsed laser deposition technique on (100) oriented
10 cubic yttria stabilized zirconia (YSZ) substrates from a stoichiometric target of GFO
11 (Ga:Fe = 1). Film growth was carried out using KrF excimer laser ($\lambda=248$ nm) in an
12 oxygen ambient ($pO_2 \sim 0.53$ mbar) at a substrate temperature of 800°C using a laser
13 fluence of 2 J/cm^2 at a laser repetition rate of 3 Hz. As-grown films were subsequently
14 cooled slowly to room temperature under the same ambient pressure. X-ray diffraction of
15 the films was performed using a high resolution PANalytical X'Pert PRO MRD thin film
16 diffractometer using $\text{CuK}\alpha$ radiation. Ellipsometric measurements were carried out using
17 HORIBA JOBIN-YVON spectroscopic ellipsometer (SE) over the energy range of 0.8-
18 4.2 eV with an incidence angle of 70° .

19 For calculations of the optical properties of the ground state structure of GFO, [14,
20 24] we employed density functional theory (DFT+U) [26] using pseudopotential based,
21 Vienna *Ab-initio* simulation package (VASP) [27] and applied the projector augmented
22 wave method (PAW) [28]. Kohn-Sham equation [29] was solved using the generalized
23 gradient approximation (GGA+U) method ($U = 5$ eV, $J = 1$ eV) with the optimized
24 version of Perdew-Burke-Ernzerhof functional for solids (PBEsol). [30] For calculations,
25 we included three valence electrons of Ga ($4s^2 4p^1$), eight for Fe ($3d^7 4s^1$) and six for O
26 ($2s^2 2p^4$) ions. A plane wave energy cut-off of 550 eV was used. We used Monkhorst-
27 Pack [31] $4 \times 4 \times 4$ mesh in our calculations. To check the robustness of our calculations,
28 we also repeated some of our calculations using LSDA+U with identical U and J values
29 used in GGA+U calculations. Further, we employed full-potential based WIEN2k code
30 using TB-mBJ functional [32] to substantiate our pseudopotential based calculations.
31 Recently developed TB-mBJ functional [32] has been reported to reproduce the
32 experimental band gap quite accurately in a number of systems [32].

33 34 **Results and Discussion:**

35 36 **(a) Ellipsometric determination of the optical properties of GaFeO_3 thin films**

37 Fig. 1(a) shows the XRD spectrum of an as-grown GFO film over the 2θ range from 15°
38 to 85° showing (010)-type reflections of orthorhombic structure of GFO (shown in the
39 right inset), indicating epitaxial nature of the film. Absence of any other peaks in the
40 XRD spectra suggests that the film is free of any impurity phase. The out-of-plane lattice
41 parameter ($b = 9.3973$ Å) estimated from the peak positions shows a close agreement
42 with the previously reported XRD data on single crystal GFO ($b = 9.3950$ Å) [23]
43 indicating that the film is fully relaxed along b -direction. However, in-plane lattice
44 parameters are strained by ~ 1.63 % due to a mismatch with the substrate lattice
45 parameters. Presence of large strain is also depicted by noticeably large full width half

1 maximum (FWHM) of the rocking curve analysis of (040) peak, as shown in the left inset
 2 of Fig. 1(a).

3 Ellipsometric measurements provide a relative change of the amplitude and phase
 4 of linearly polarized monochromatic light reflected from the sample surface, with respect
 5 to the incident light. Ellipsometric parameters, ψ and Δ are related to sample's optical and
 6 structural properties by: $\frac{R_p}{R_s} = \tan \psi \cdot e^{i\Delta}$ where, R_p and R_s are the coefficients of reflection
 7 of polarized light parallel and perpendicular to the plane of incidence, respectively. [33]
 8 Ellipsometric parameters, ψ and Δ can further be used to describe two intensity
 9 parameters termed as:

$$10 \quad \begin{aligned} IS &= \sin 2\psi \sin \Delta \\ IC &= \cos 2\psi \cos \Delta \end{aligned} \quad (1)$$

11 In the present work, we have used a three layer model, as shown in the inset of
 12 Fig. 1(b), to analyze the ellipsometric data. The layer, labeled as L2 represents the actual
 13 film while L1 and L3 take into account the substrate-film interface and film roughness,
 14 respectively. The dispersion in L1 consists of 50 % film and 50 % substrate while that in
 15 and L3 consists of 50 % film and 50 % void. In order to derive the complex dielectric
 16 function and other optical properties from our ellipsometry data, we used Tauc-Lorentz
 17 (TL) model [34] in which the imaginary part of the dielectric function is given by:

$$18 \quad \begin{aligned} \epsilon'' &= \frac{1}{E} \cdot \frac{AE_0\Gamma(E - E_g)^2}{(E^2 - E_0^2)^2 + (\Gamma E)^2} \quad \text{for } E > E_g \\ &= 0 \quad \text{for } E \leq E_g \end{aligned} \quad (2)$$

19 where A is amplitude factor which is a function of material density and the momentum
 20 matrix element, E_0 is peak transition energy corresponding to Penn gap, Γ is broadening
 21 parameter related to crystallite size [35] and E_g is the band gap energy. To take into
 22 account the substrate effect, we assigned a three oscillator Tauc-Lorentz model [34]
 23 which described the dispersion of a bare substrate satisfactorily. Fig. 1(b) shows the
 24 experimental data (symbols) and corresponding fits (solid lines) of IS and IC of the GFO
 25 film. Our ellipsometry data showed a surface roughness of ~ 21 nm and a film thickness
 26 of ~ 85 nm which were consistent with our atomic force microscopy (AFM) and surface
 27 profilometer measurements. The fitting parameters are listed in the Fig. 1(b)

29 **(b) Comparison of ellipsometric data with the ground state properties with no** 30 **external perturbation**

31 Ellipsometry data along with the results of the density functional calculations of real (ϵ')
 32 and imaginary (ϵ'') components of dielectric function are plotted in Fig. 2 (a). Simulation
 33 of the ellipsometric data using Tauc-Lorentz (TL) model [34] yielded an energy band gap,
 34 E_g , of $\sim 2.28 \pm 0.08$ eV, consistent with our ground state electronic structure calculations
 35 [14, 24] but lower than the previous experimental data. [16] The plots of ϵ'' versus photon
 36 energy show that absorption in our samples begins at ~ 2 -2.5 eV. For a clear visualization
 37 of the absorption edge, absorption coefficient (α) is plotted semi-logarithmically, as
 38 shown in Fig. 2(b). Further, initial part of the absorption spectra beyond the band gap
 39 shows a quadratic dependency on incident photon energy (solid line in of Fig. 2(b))
 40 indicating GFO to be an indirect band gap semiconductor. From the fitting of the

1 absorption spectra, the indirect band gap was estimated as $E_g \sim 2.28 \pm 0.02$ eV which is
2 in excellent agreement with the one obtained from the simulation of the ellipsometric data
3 using TL model. However, this is in contrast with our earlier calculations [14] on the
4 ground state structure where we found that direct and indirect band gaps in GFO are
5 identical. We find that below the band edge, the values of ϵ'' and k are zero while ϵ' and
6 refractive index (n) possess dispersive behavior, as a function of photon energy, as shown
7 in the inset of Fig.2 (b). To understand the origin of the experimental optical behavior in
8 GFO, we performed first-principles studies using both pseudopotential (GGA+U and
9 LSDA+U) and full-potential (TB-mBJ) based approaches. A comparison, as shown in Fig.
10 2(a), demonstrates that while our experimental data is consistent with a previous report
11 on single crystal GFO, [25] our LSDA+U, GGA+U and TB-mBJ calculations do not
12 reproduce the experimental data very well. While LSDA+U and GGA+U underestimate
13 the band gap (red shift of the absorption edge with respect to the experiment) TB-mBJ
14 yields a good agreement of the band gap with the experiment. The difference in the
15 intensities between the experimental data and the calculated profiles could be attributed
16 to a number of factors namely, sample quality, temperature, difference between
17 experimental and the ground state crystal and magnetic structures, type of approximation
18 scheme used in the first-principles calculations and the type of broadening used in the
19 experimental and calculated data. [36]

20 Overall, since our GGA+U profile matched best (among all the calculated results)
21 with the experimental data, subsequent discussions are limited to GGA+U results only.
22 We first calculated the ground state dielectric properties, ϵ' and ϵ'' , along the three
23 principal crystallographic directions as plotted in Fig. 2(c). Here, we observe that the
24 optical constants of GFO are anisotropic in nature, a feature consistent with the
25 orthorhombic symmetry of the unit cell and also supported by previous report on GFO
26 single crystal. [25] Further, we also identified the major features (peaks) in the ϵ'' plot
27 which, in case of insulators like GFO, originate primarily from the inter-band transitions,
28 *i.e.*, from valence (VB) to conduction (CB) bands. We computed the electronic band
29 structure and density of states using GGA+U to identify the transitions responsible for the
30 optical activities in GFO and the results are shown in Fig. 3 (a) and (b). The allowed
31 optical transitions are labeled in the band structure. The density of states plot shows that
32 the upper most part of the VB, -2 eV to 0 eV, is dominated by O 2p states with rather
33 suppressed Fe 3d and Ga 4p states. On the other hand, the lower part of CB is mostly
34 occupied by Fe 3d bands with a subdued presence of O 2p and Ga 4s states. Thus, we can
35 conclude that the optical transitions labeled in Fig. 2(c) and Fig. 3(a) involve transitions
36 from O 2p to Fe 3d states which is further corroborated by the experimental work of
37 Kalashnikova *et al.* [25] Small occupation of O 2p states near the conduction band
38 minimum indicates that GFO has a significant ionic character which is substantiated by
39 our previous charge density and electron localization function (ELF) calculations [14]
40 interpreting negligible ELF values at Fe sites as a signature of complete charge transfer
41 between Fe and O.

42 O2p-Fe3d electronic transition could further be elucidated using crystal field
43 theory. Within the regular FeO₆ octahedral crystal environment with O_h point symmetry,
44 five Fe 3d and 18 O 2p atomic orbitals construct Fe 3d-O 2p bonding and antibonding
45 molecular orbitals (MO), e_g and t_{2g} , respectively. In addition, O2p π - O2p π hybridization
46 leads to oxygen nonbonding orbitals are $t_{1g}(\pi)$, $t_{2u}(\pi)$, $t_{1u}(\pi)$, $t_{1u}(\sigma)$ and $a_{1g}(\sigma)$. [37] The

1 relative energy states of these orbitals play a pivotal role in determining O 2p - Fe 3d
2 transitions responsible for the observed optical activity of GFO. Selection rule allows six
3 transitions in the strong absorption region (energy level ≥ 3.0 eV): ${}^6A_{1g} \rightarrow {}^6T_{1u}$ related to
4 one electron transition between $t_{2u}(\pi)$, $t_{1u}(\pi)$, $t_{1u}(\sigma)$ and t_{2g} and e_g levels, [38, 39].
5 However, MOs in the O_h point symmetry further split due to non-cubic (D_{2h}) crystal field
6 distortion in GFO and such symmetry lowering in the actual crystal environment would
7 lift some of the restrictions of the transitions leading to the appearance of many more
8 transitions, as shown by several peaks in Fig. 2(c).
9

10 (c) Effect of external perturbations on the ground state optical properties

11 The discussion in the previous section was based on the assumption that GFO has
12 antiferromagnetically ordered bulk structure with no site disorder at 0 K. These
13 assumptions are often challenged because materials in thin film forms experience
14 substantial substrate induced strain leading to structural distortion. Consequently, such
15 distortions give rise to modifications in the inter-ionic bond spacing and angles affecting
16 the electronic structure and materials properties. For example, a number of ferroelectric
17 oxides have been reported to demonstrate large variations in the polarization upon
18 application of epitaxial strain. [40] Moreover, experimental structure of GFO is shown to
19 possess significant cation site disorder among Ga and Fe sites driven by their similar
20 ionic sizes [21, 23] which is also ignored in the ground state calculation. In the following
21 sections, we introduce these structural changes in the ground state structure and compare
22 the results of GGA+U calculations with the experiments.
23

24 (i) Effect of epitaxial strain

25 First, we analyze effect of epitaxial strain on the optical properties and electronic band
26 structure of GFO. The range of strain chosen is on the basis of present and past
27 experiments [16] where choice of substrate leads to a misfit strain of the order of $\sim 1-3$ %.
28 Here, first we plot the real and imaginary parts of dielectric constant (ϵ' and ϵ'') as a
29 function of incident photon energy (Fig. 4(a)) with varying magnitudes of strain. We find
30 that the nature of the ϵ' plot remains almost identical to that of ground state structure for
31 strain = ± 1 %. Further ϵ'' plot shows that the peak at ~ 3.8 eV remains similar for the
32 ground state and -1% strain and it splits into two peaks for +1% strain with splitting
33 further getting pronounced upon increasing the strain to +3%. However, the low energy
34 regions of the ϵ'' spectra remain identical with no noticeable shift of the absorption edge
35 with the application of strain. These observations indicate that the application of epitaxial
36 strain on the ground state structure alone does not improve the agreement between the
37 experimental and calculated dielectric spectra in GFO.

38 In addition, the refractive index (at 3 eV) increased linearly with increasing
39 applied strain. To identify the origin of such strain dependent optical activity, we
40 compared the electronic structure obtained at 0% and +3% strains. These showed that the
41 PDOS of Fe 3d states slightly shifted towards higher energy in the conduction band with
42 the application of tensile strain which is attributed to the reduction of some of the Fe-O
43 bond lengths resulting in overlapping wavefunctions and consequent hybridization.
44
45
46

1 (ii) Effect of cation site disorder

2 So far, our calculations were limited to the ground state antiferromagnetic structure of
3 GFO assuming that there was no cation site disorder. However, the actual structure of
4 GFO always contains cation site disorder driven by quite similar ionic sizes of Ga and Fe.
5 [21, 23] Our previous work demonstrated that site disorder between Fe2 and Ga2 sites is
6 most probable followed by Fe1 and Ga1 sites. [24] We incorporated these Ga-Fe site
7 disorders, one at a time, to study their effect on the optical response in GFO in the
8 unstrained structure. Since the structure of GFO contains four equivalent ions of each
9 cation, exchange of ionic sites between one Fe1/Fe2 to one Ga1/Ga2 would lead to a 25%
10 site disorder in the structure. The degree of disorder, particularly Fe2-Ga2 disorder
11 conceived here is similar to the experimental structure. [21] Calculated dielectric
12 constants of GFO consisting of cation site disorder are plotted in Fig. 4(b) along with
13 those obtained on thin film samples, and the ordered ground state structure. A close
14 inspection of the ϵ'' spectra near the absorption edge reveals that while Fe1 to Ga1 site
15 interchange does not affect the position of the absorption edge with respect to that of the
16 ground state structure, Fe2 to Ga2 site interchange imparts a leftward shift indicative of a
17 reduction in the band gap. Further, we also find that with Fe1-Ga1 site interchange, the
18 peak in the ϵ'' plot at ~ 2.86 eV (peak A in Fig. 2(c)) is suppressed whereas it almost
19 vanishes for Fe2-Ga2 interchanged structure. On the other hand, the peak at ~ 2.70 eV in
20 the ϵ' spectra of the ordered ground state structure is effectively flattened for Fe2-Ga2 site
21 interchange resulting in a remarkably closer resemblance of the calculated with the
22 experimental data reported by Kalashnikova *et al.* [25] and a much improved match with
23 our experimental results. The observed similarities between the experimental and Fe2-
24 Ga2 site interchanged spectra further substantiate the fact that GFO has inherent cation
25 site disorder with a predominant Fe2-Ga2 site exchange.

26 Subsequent calculations of electronic band structure and site projected density of
27 states (Fig. 3(c) and (d)) reveal that the evolution of band structure upon incorporating the
28 site disorder differs significantly from that of the ground state band structure. We find
29 that the band gap of site-interchanged GFO is of indirect type ($E_g \sim 1.82$ eV), consistent
30 with our ellipsometry measurement. The difference in magnitude could be attributed to
31 the GGA method used for the band structure calculation. Site projected DOS plots show
32 that there is a shift of Fe2 3d states towards lower energy which is translated into the
33 down shift of the bands in the band structure and is responsible for the observed red shift
34 of the absorption edge in Fig. 4(b). The reduction of the band gap upon Fe2-Ga2 site
35 interchange is related to the reduction in some of the Fe2-O bond lengths (in the
36 disordered structure) with respect to the corresponding Ga2-O bonds (in the ground state
37 structure) and variation of crystal environment upon imparting the disorder. Reduction of
38 the bond length would induce stronger hybridization and consequently widen the band
39 dispersion leading to a reduction in the band gap.

40 Disorder induced variation of crystal environment could further be studied by a
41 comparison of electron localization function (ELF) of the ground state structure and the
42 Fe2-Ga2 site interchanged structure (not shown here). While finite ELF values between
43 Ga1-O and Ga2-O indicate significant covalency, complete charge transfer between Fe2
44 and O sites is evident from zero ELF value at Fe2 site and across Fe2-O bonds. Thus site
45 disorder modifies the ELF mapping within the unit cell and consequently the crystal

1 environment. Such variation of the crystal environment is believed to be responsible for
2 the evolution of electronic structure and consequent optical spectra in the disordered GFO.

3 4 **(iii) Combined effects of site-disorder and epitaxial strain**

5 Finally, to completely mimic the experimental scenario in GFO epitaxial thin films, we
6 applied tensile epitaxial strain to Fe₂-Ga₂ site disordered structure (as discussed in
7 section (ii)) and calculated the optical properties and then compared the results with our
8 experimental data of thin films (Fig. 4(c)). Here we observe that the agreement between
9 the experiment and the calculations further improves significantly upon application of
10 tensile strain on the structure with 25% Fe₂-Ga₂ cation site disorder. While the band gap
11 calculations suffer from inherent limitation of LDA and GGA techniques and hence are
12 unreliable, the calculated spectra obtained upon applying tensile strain on Fe₂-Ga₂ site
13 disordered GFO is remarkably similar to the experimentally obtained dielectric function
14 as shown in Fig. 4(c). The difference in the absolute intensities can be attributed to
15 various extrinsic parameters such as the sample quality, temperature etc. The electronic
16 structure of the modified structure of GFO would have contributions from the above two
17 effects described in 3(b) and 3(c) where disorder drives the Fe 3d bands of the Fe₂ ion at
18 the Ga₂ site to shift downward while tensile strain alters the cation-oxygen bond-lengths
19 and angles which in turn alter the positions of the electronic states. We further compared
20 the experimental optical constants with these calculations over the experimental
21 measurement domain as shown in Fig. 5. In Fig 5(a), we show the calculated and
22 experimental results for n and k which match well with each other. It is found that
23 experimentally determined n starts with a finite value ($n \sim 2.1$) and then slowly increases
24 with energy showing a peak ($n \sim 2.5$) at ~ 3 eV. On the other hand, the calculated spectra
25 show the position of this peak at slightly lower energy due to underestimation of the band
26 gap by GGA+U method. The peak in n spectra can be attributed to the beginning of
27 absorption in the material triggered by transition from valence band O 2p to conduction
28 band Fe 3d state. On the other hand, the result for k starts with zero value and then
29 begins to increase at energy corresponding to the band gap. Since our calculated gap is
30 lower compared to the experimental gap, the experimental curve starts to rise at higher
31 energy. However, calculated spectra could be appropriately scaled (shifted by a constant
32 energy), to yield minimum qualitative mismatch of the overall profile between calculated
33 and experimental spectra. Magnitudes of n and k show a clear departure for the
34 experiment and calculations, attributed to the factors such as sample quality, temperature
35 etc. as mentioned before. Reflectivity (R) spectra in Fig. 5(b), shows an initial gradual
36 increase followed by a peak ($R \sim 0.19$) near the absorption edge which is consistent with
37 the absorption spectra, also shown in Fig. 5(b). Again, the difference between the
38 calculated and the experimental R spectra could be attributed to the band gap
39 underestimation by GGA+U calculations. Optical conductivity, as shown in Fig. 5(c),
40 demonstrates an onset above 2 eV for both experiment (~ 2.5 eV) and calculation (~ 2.1
41 eV) and level off to values, $7500 \Omega^{-1}\text{cm}^{-1}$ and $13000 \Omega^{-1}\text{cm}^{-1}$ at 4 eV for experimental
42 and calculated spectra, respectively.

43 44 **(iv) Effect of off-stoichiometry**

45 Since GFO has large compositional tolerance, [22] it would be of interest to examine the
46 effect of off-stoichiometric Ga:Fe ratio on the optical properties and consequent changes

1 in the electronic structures. This is important because it results in an imbalance in the
2 cation site occupation between Fe and Ga and its effects are manifested in the magnetic
3 behavior of GFO [22]. In this context, we have considered two cases: first, considering
4 substitution of one Ga ion at Ga2 site by one Fe ion at Fe2 site and second, considering
5 substitution of two Ga ions at Ga2 sites by two Fe2 site ions. These scenarios resemble
6 two Fe-excess compositions $x = 1.125$ and $x = 1.25$ in $\text{Ga}_{2-x}\text{Fe}_x\text{O}_3$, well within the
7 experimentally obtained single phase domain of GFO. [22] Subsequently, we relaxed the
8 two structures and computed the optical properties and the electronic structures. Here, we
9 have not included the site disorder allowing us to exclusively investigate the effect of off-
10 stoichiometry.

11 It was found that the electronic band structure and the density of states (plots not
12 shown) calculations of these off-stoichiometric compositions show similar effects as
13 observed for the disordered GFO. It was observed that with increasing Fe content, Fe ions
14 substituting Ga2 sites would have Fe 3d states at increasingly low energies resulting in a
15 monotonic decrease in the band gap. Lowering of crystal symmetry due to doping further
16 induces band splitting of Fe 3d band in these cases. Resulting modifications in the
17 electronic structures thus, affect the optical spectra for compositions having excess Fe
18 content. Fig. 6(a) shows the yy component of real and imaginary parts of dielectric
19 constant tensors with different stoichiometry *viz.*, $x = 1.0$, $x = 1.125$ and $x = 1.25$. We
20 observe that with increasing Fe content the fundamental absorption edge shifts towards
21 lower energy consistent with the previous experimental observations on single crystal
22 [25] and our band structure calculations which show a reduction in the band gap with
23 increasing Fe content (x). Moreover, the intensity of dielectric function increases with
24 increasing Fe content.

25 **(v) Effect of hydrostatic pressure**

26 Finally, we take into account the structural distortion which can induce the instability
27 leading to phase transformation in a few systems with significant magneto-structural
28 coupling. [41, 42] Such distortion which can be brought about by applying hydrostatic
29 stress has also been reported to alter the magnetic behavior in GFO owing to the presence
30 of magneto-structural coupling. [24] Here, we study the evolution of optical constants of
31 GFO as a function of distortion induced by hydrostatic stress. The evolution of yy
32 component of real and imaginary parts of dielectric constants as a function of application
33 of hydrostatic pressure is shown in Fig. 6(b). The figure shows that with increasing
34 hydrostatic pressure, the position of the first peak in the ϵ'' spectra remains almost
35 identical, while the peak at 3.78 eV tends to shift towards higher energy. An additional
36 peak also appears which is marked with the vertical arrow beyond 20 GPa. The evolution
37 of such optical behavior has its origin in the electronic structure as we explain below.
38 With increasing hydrostatic pressure, since the structure is distorted as the bond lengths,
39 in general, are decreased. As a result, there is a growing tendency of the wave functions
40 of the adjacent ions to overlap with each other. Consequently, the energy levels shift in a
41 repulsive manner which is reflected in the observed optical behavior. Such modification
42 of electronic structure of GFO upon application of pressure has been explained in our
43 previous work. [24] The inset of Fig. 6 (b) shows yy component of the refractive index
44 (n) as a function of applied pressure exhibiting a gradual fall at the incident photon
45

1 energy of 3 eV. Thus, this study qualitatively demonstrates the presence of a coupling
2 between the optical and the structural parameters.

3 4 **IV. Conclusions**

5
6 In summary, we have performed ellipsometry studies on epitaxial GaFeO₃ thin films and
7 have compared the dielectric response and other optical constants with our density
8 functional calculations using different approximation schemes with GGA+U showing the
9 best agreement with the experiments. The origin of optical activities in GFO is identified
10 as transition from O 2p to Fe 3d states. We find that the inclusion of site disorder, off-
11 stoichiometry, epitaxial strain and hydrostatic pressure influence the optical properties
12 due to shifting of Fe 3d state. We observe that incorporation of the cation site disorder
13 into GFO lattice renders it to become an indirect band gap semiconductor, consistent with
14 the experimental observations. Further, the cation site disorder also brings about a
15 significant reduction in the electronic band gap with respect to that of the ground state
16 structure of GFO. Interestingly, we find that inclusion of site disorder and epitaxial strain
17 into the ground state structure significantly improves the agreement between calculated
18 and experimental results clearly illustrating that gallium ferrite contains inherent cationic
19 site-disorder.

20 21 **Acknowledgements**

22 The work was supported by Department of Science and Technology, Govt. of India
23 through project number SR/S2/CMP-0098/2010. Authors thank Prof. Y.N. Mohapatra,
24 SA thanks NPL for the J C Bose Fellowship.

25 26 **References**

- 27
28 [1] Teowee G, Boulton JM, Uhlmann DR 1998 *Int. Ferroelectrics* **20** 39.
29 [2] Murphy TE, Chen D, Phillips JD 2004 *Appl. Phys. Lett.* **85** 3208.
30 [3] Muralt P 1996. *ISAF '96., Proceedings of the Tenth IEEE International*
31 *Symposium* **1** 145.
32 [4] Polla DL 1992 *ISAF '92., Proceedings of the Eighth IEEE International*
33 *Symposium* 127.
34 [5] Li S, Lin Y-H, Zhang B-P, Nan C-W, Wang Y 2009 *J. Appl. Phys.* **105** 056105.
35 [6] Brody P, Crowne F 1975 *J. Electron. Mater.* **4** 955.
36 [7] von Baltz R, Kraut W 1980 *Phys. Lett. A* **79** 364.
37 [8] Pintilie L, Alexe M, Pintilie I, Botila T 1996 *Appl. Phys. Lett.* **69** 1571.
38 [9] Yang SY, Martin LW, Byrnes SJ, Conry TE, Basu SR, Paran D, Reichertz L,
39 Ihlefeld J, Adamo C, Melville A, Chu YH, Yang CH, Musfeldt JL, Schlom DG,
40 Ager JW, Iii, Ramesh R 2009 *Appl. Phys. Lett.* **95** 062909.
41 [10] Choi WS, Chisholm MF, Singh DJ, Choi T, Jellison GE, Lee HN 2012 *Nat.*
42 *Commun.* **3** 689.
43 [11] Liu P-L, Wang J, Zhang T-Y, Li Y, Chen L-Q, Ma X-Q, Chu W-Y, Qiao L-J
44 2008 *Appl. Phys. Lett.* **93** 132908.
45 [12] Singh DJ, Seo SSA, Lee HN. 2010 *Phys. Rev. B* **82** 180103.
46 [13] Guo S-D, Liu B-G 2011 *J. Appl. Phys.* **110** 073525.

- 1 [14] Roy A, Mukherjee S, Gupta R, Auluck S, Prasad R, Garg A 2011 *J. Phys.:*
2 *Condens. Matter* **23** 325902.
- 3 [15] Roy A, Prasad R, Auluck S, Garg A 2010 *J. Phys.:* *Condens. Matter* **22** 165902.
- 4 [16] Sun ZH, Dai S, Zhou YL, Cao LZ, Chen ZH 2008 *Thin Solid Films* **516** 7433.
- 5 [17] Jung JH, Matsubara M, Arima T, He JP, Kaneko Y, Tokura Y 2004 *Phys. Rev.*
6 *Lett.* **93** 037403.
- 7 [18] Kida N, Kaneko Y, He JP, Matsubara M, Sato H, Arima T, Akoh H, Tokura Y
8 2006 *Phys. Rev. Lett.* **96** 167202.
- 9 [19] Ogawa Y, Kaneko Y, He JP, Yu XZ, Arima T, Tokura Y 2004 *Phys. Rev. Lett.* **92**
10 047401.
- 11 [20] Kundaliya DC, Ogale SB, Dhar S, McDonald KF, Knoesel E, Osedach T, Lofland
12 SE, Shinde SR, Venkatesan T. 2006 *J. Magn. Magn. Mater.* **299** 307.
- 13 [21] Arima T, Higashiyama D, Kaneko Y, He JP, Goto T, Miyasaka S, Kimura T,
14 Oikawa K, Kamiyama T, Kumai R, Tokura Y 2004 *Phys. Rev. B* **70** 064426.
- 15 [22] Mukherjee S, Ranjan V, Gupta R, Garg A. 2012 *Solid State Commun.* **152** 1181.
- 16 [23] Mukherjee S, Garg A, Gupta R 2011 *J. Phys.:* *Condens. Matter* **23** 445403.
- 17 [24] Roy A, Prasad R, Auluck S, Garg A 2012 *J. Appl. Phys.* **111** 043915.
- 18 [25] Kalashnikova A, Pisarev R, Bezmaternykh L, Temerov V, Kirilyuk A, Rasing T.
19 2005 *JETP Lett.* **81** 452.
- 20 [26] Jones RO, Gunnarsson O 1989 *Rev. Mod. Phys.* **61** 689.
- 21 [27] Kresse G, Joubert D 1999 *Phys. Rev. B* **59** 1758.
- 22 [28] Blöchl PE 1994 *Phys. Rev. B* **50** 17953.
- 23 [29] Kohn W, Sham LJ 1965 *Phys. Rev.* **140** A1133.
- 24 [30] Perdew JP, Ruzsinszky A, Csonka G, aacute, bor I, Vydrov OA, Scuseria GE,
25 Constantin LA, Zhou X, Burke K 2008 *Phys. Rev. Lett.* **100** 136406.
- 26 [31] Monkhorst HJ, Pack JD 1976 *Phys. Rev. B* **13** 5188.
- 27 [32] Tran F, Blaha P 2009 *Phys. Rev. Lett.* **102** 226401.
- 28 [33] Azzam RMA, Bashara NM. Ellipsometry and Polarized Light. Amsterdam:
29 North-Holland, 1977.
- 30 [34] Jellison JGE, Modine FA 1996 *Appl. Phys. Lett.* **69** 371.
- 31 [35] Feng GF, Zallen R 1989 *Phys. Rev. B* **40** 1064.
- 32 [36] Skorodumova NV, Ahuja R, Simak SI, Abrikosov IA, Johansson B, Lundqvist BI
33 2001 *Phys. Rev. B* **64** 115108.
- 34 [37] Pisarev RV, Moskvina AS, Kalashnikova AM, Rasing T 2009 *Phys. Rev. B* **79**
35 235128.
- 36 [38] Likhtenshteĭn AI, Moskvina AS, Gubanov VA 1982 *Sov. Phys. Solid State* **24** 2049.
- 37 [39] Usachev P, Pisarev R, Balbashov A, Kimel A, Kirilyuk A, Rasing T 2005 *Phys.*
38 *Solid State* **47** 2292.
- 39 [40] Ederer C, Spaldin NA 2005 *Phys. Rev. Lett.* **95** 257601.
- 40 [41] Lee JH, Rabe KM 2010 *Phys. Rev. Lett.* **104** 207204.
- 41 [42] Singh DJ, Pickett WE 1998 *Phys. Rev. B* **57** 88.
- 42
43

1 **Figure Captions**

2
3 Fig. 1 (a) XRD spectrum of a pulsed laser deposited GFO thin film showing (010)
4 orientation (the left inset shows the rocking curve of (040) peak and the right inset shows
5 a schematic of the orthorhombic unit cell of GFO); (b) fitting of ellipsometry data using
6 Tauc-Lorentz model with fit parameters listed inside the plot (inset shows the three layer
7 model used for simulation).

8
9 Fig.2 (a) Real (ϵ') and imaginary (ϵ'') parts of dielectric function determined
10 experimentally and theoretically and compared with the literature; (b) experimentally
11 determined absorption coefficient (α) showing the absorption edge (inset plots dispersion
12 of experimentally computed refractive index (n) and extinction coefficient (k)) and (c) ϵ' ,
13 ϵ'' spectra along principal crystallographic directions corresponding to the ground state
14 structure of GFO calculated using GGA+U method, plotted as a function of incident
15 photon energy

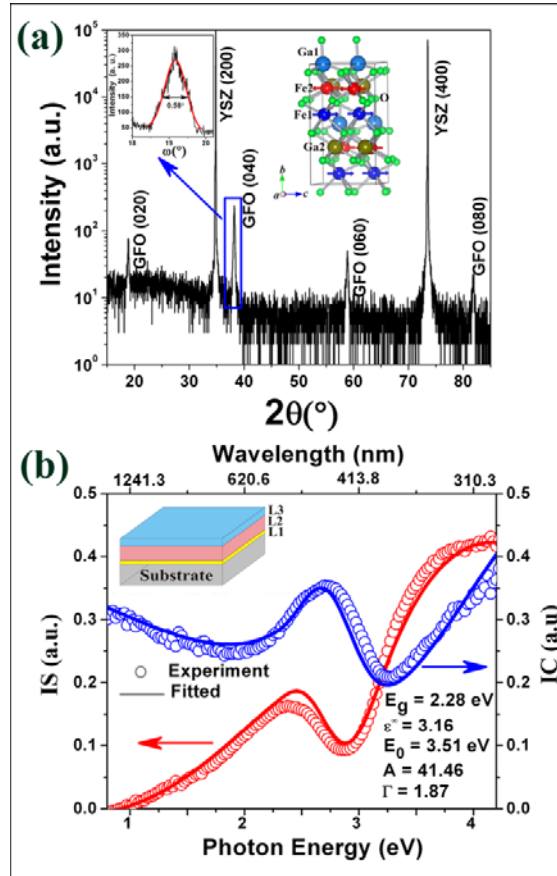
16
17 Fig.3 (a) Electronic band structure of the ground state structure of GFO with arrows
18 indicating the interband transitions responsible for the evolution of the peaks in the ϵ''
19 spectra shown in Fig.1 (c); (b) total and partial density of states of ground state structure
20 of GFO; (c) comparison of band structures of the ground state and Fe2-Ga2 site disorder
21 structures and (d) total and partial density of states of Fe2-Ga2 site disordered structure.

22
23 Fig.4 Real (ϵ') and imaginary (ϵ'') components of dielectric function plotted as a function
24 of incident photon energy obtained experimentally and theoretically showing effect of (a)
25 epitaxial strain, (b) site disorder and (c) epitaxial strain and Fe2-Ga2 site disorder.

26
27 Fig.5 Comparison of experimentally determined optical constants with Fe2-Ga2 site
28 interchanged structure with tensile strain of 3 %.

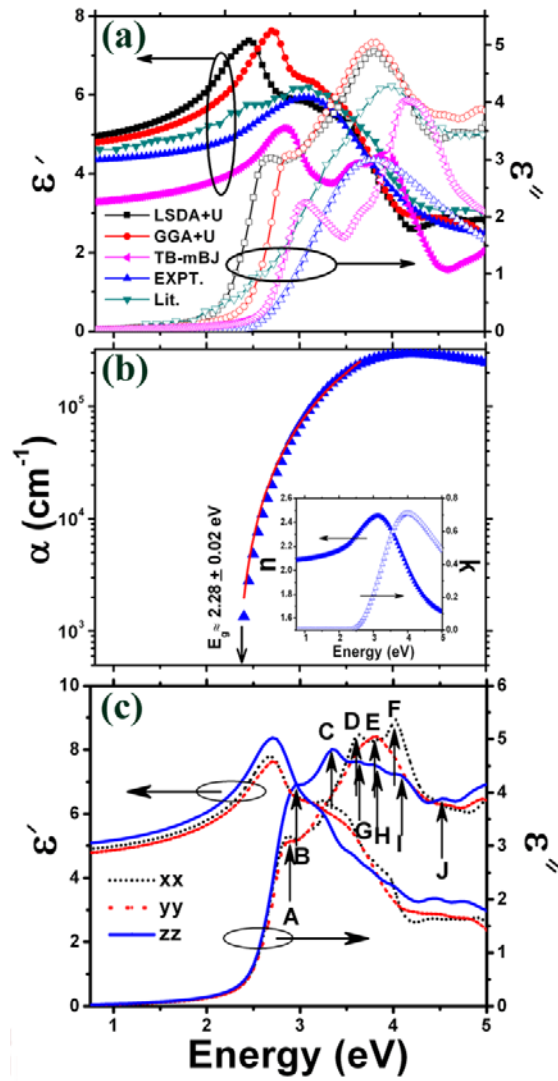
29
30 Fig.6 Effect of (a) off-stoichiometry and (b) hydrostatic pressure on the ϵ' , ϵ'' spectra of
31 GFO, inset shows the variation of refractive index at 3 eV as a function of applied
32 hydrostatic pressure.

1
2
3



4
5
6
7
8

Fig. 1 Roy et al



1
2 Fig. 2 Roy et al
3

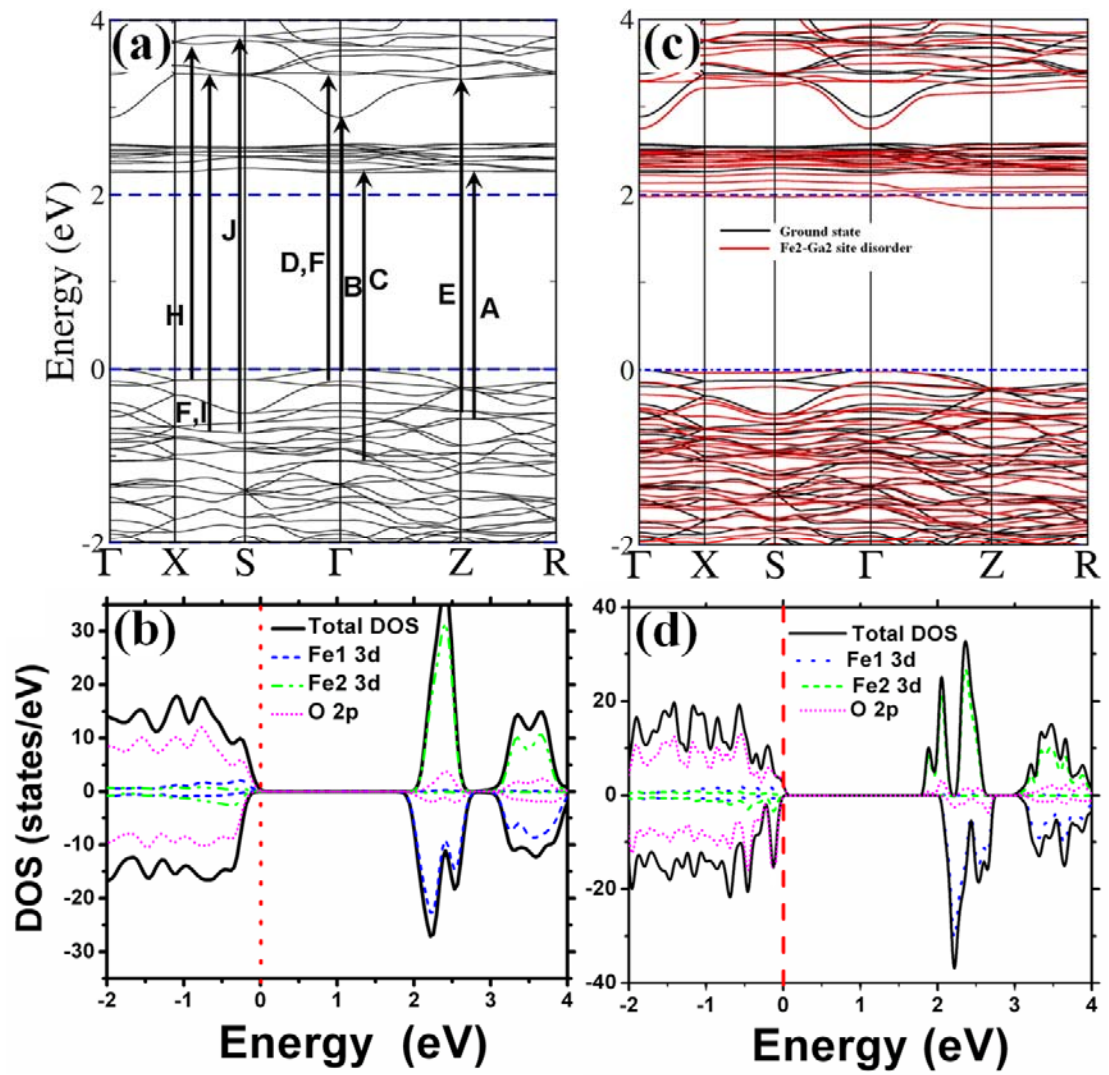
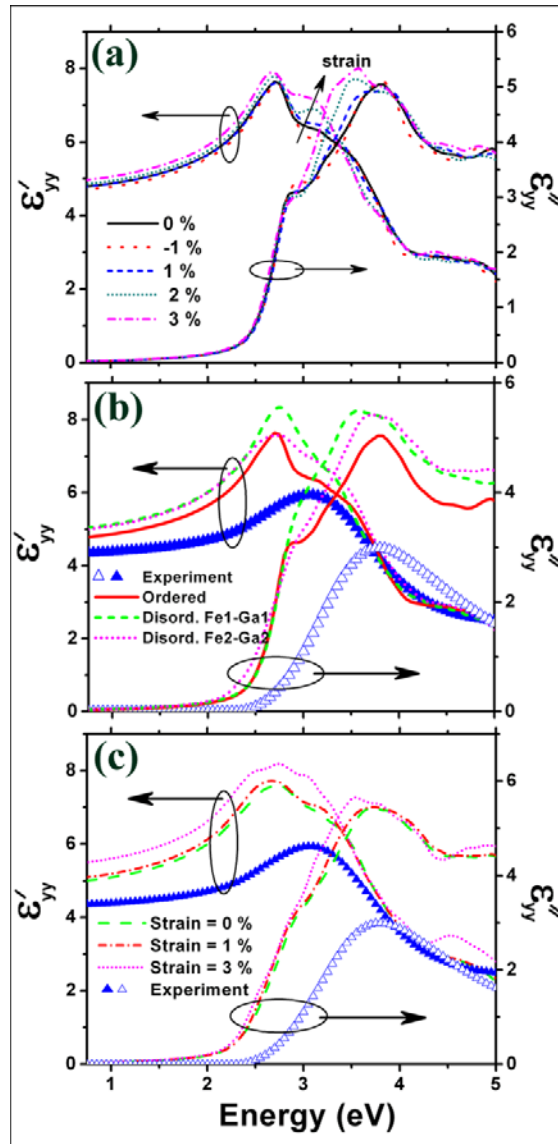


Fig.3 Roy et al

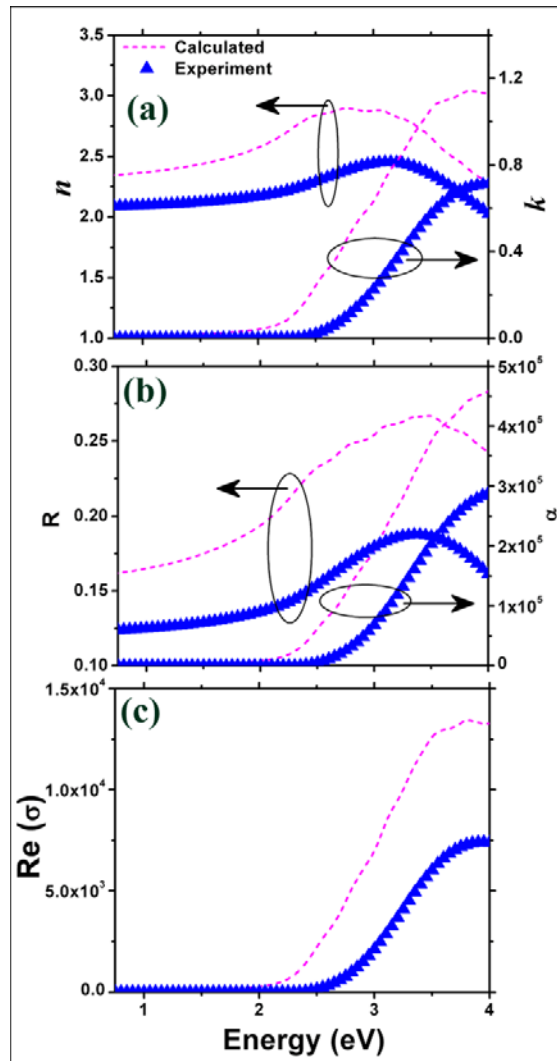
1
2
3
4
5
6
7
8
9
10
11
12
13
14



1
2
3
4
5
6
7
8
9
10
11
12
13
14
15

Fig.4 Roy et al

1



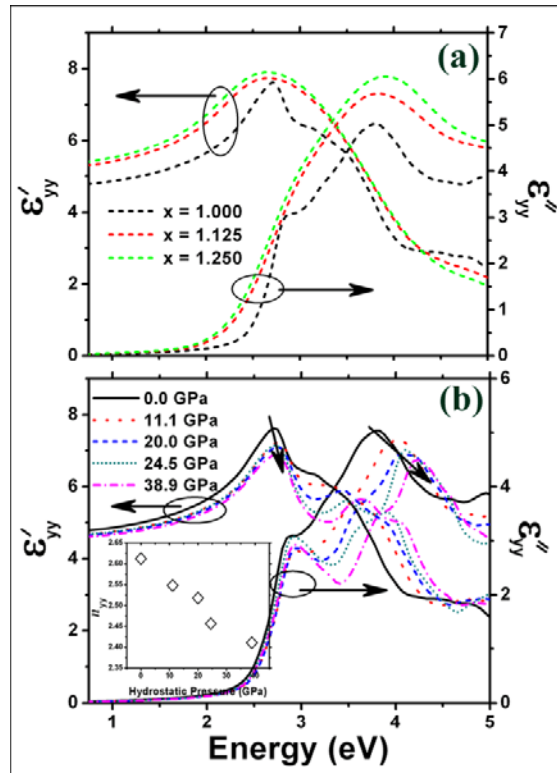
2

3

4

5

Fig.5 Roy et al



1
2
3
4
5
6
7
8
9

Fig. 6 Roy et al